

Networks of coupled random lasers with spatially localized feedback

Niccolò Caselli^{1†*}, Antonio Consoli^{1,2#}, Angel Maria Mateos¹, Cefe López^{1§}

Light interference in strongly disordered photonic media can generate random lasers capable to amplify clumps of modes in an unpredictable fashion. The ease of fabrication, along with the low coherence and small linewidths, placed random lasers as emerging, efficient speckle-free light sources and a means to achieve spectral super-resolution. At the verge of becoming a mature and accessible technology, their complex systems nature still furnishes the opportunity to unveil fundamental physics, since they can act as elements of optical network architectures. No experimental studies have analysed the optical interaction between single resonators in networks of random lasers so far. In this letter, we investigate, both experimentally and numerically, networks of random lasers based on spatially localized feedback that share common scattering centres. We prove that the emission of a single random laser can be manipulated by the action of others in the network, giving rise to sizable peak rearrangements and energy redistribution, fingerprint of mode coupling. Our findings, involving a few coupled random lasers, firmly set the basis for the study of full-grown photonic networks. Oddly, both their deep understanding and their deployment as hardware clearly point in the direction of a novel disruptive technology: artificial intelligence on photonic neural networks.

Keywords: optical networks, random laser

Introduction

Synchronization among coupled elements is a ubiquitous concept¹ used for describing the dynamics of non-linear systems arranged in complex networks^{2,3}, spanning from oscillatory mechanical modes⁴, spatiotemporal chaos in fluid dynamics⁵, synaptic neurons⁶ to interacting lasers^{7,8}. Nanophotonics has recently gained attention for mimicking both structural and functional features of neural networks by developing integrated optical circuits and coupled lasers where the non-linearity is given by the amplified light emission^{7,9}. While synchronization has been proved in systems of interacting semiconductor lasers^{10,11} little is known about the same effect in random laser (RL) architectures, which with ease can give rise to complex networks^{12–14}.

At variance with conventional lasers, RLs do not require the engineering of a high-quality cavity, since they are based on disordered media in which the feedback necessary to trigger the laser amplification is provided by strong elastic light scattering^{15–17}. Therefore, they rely on a relatively easier manufacture, which allows inexpensive devices. A RL typically presents many narrow-line modes that cannot be arranged *a priori* as in a conventional cavity laser. The resulting emission shows lower spatial coherence, furnishing speckle-free illumination¹⁸, as well as enabling spectral super-resolution¹⁹. RLs and, more generally, optical localized random modes, have found application in a large variety of fields from energy harvesting²⁰, information processing²¹ to sensing²² and tumour cell recognition²³, to name a few.

The most widespread RL implementation is based on spatially distributed feedback, where the scattering centres are randomly placed inside the optically active medium. A different configuration, called RL with spatially localized feedback, in which the scattering elements are separated from the active medium that is embedded between them, has been developed^{24,25}. Since their geometry does not vary with time, they show a stable emission that allows to disentangle the contribution when single RLs are arranged in a network. Coupling between modes has been studied in a single RL both with distributed²⁶ and localized feedback²⁵ but not between multiple RLs.

Here, we demonstrate that this modal interaction can be induced in multiple disordered resonators, giving rise to a new class of active optical networks based on RLs with spatially localized feedback. The network, defined in the plane of the gain material, is determined by several, distant, nondescript, scattering centres multiply connected by optically pumped lines. The system can be considered as a unique collective resonator in which manifold coupled oscillators are turned on at will. This is proved by the fact that revealing spectral signatures are observed at all the nodes of the network.

Numerical calculations based on coupled mode theory were carried out and predictions on the spectral redistribution induced by the interacting RL network are found in agreement with the observed synchronization behaviours. Finally, since a single network node can be used as scattering and coupling element between many resonators, more complex network architectures can be envisioned in order

¹Instituto de Ciencia de Materiales de Madrid (ICMM), Consejo Superior de Investigaciones Científicas (CSIC), Calle Sor Juana Inés de la Cruz, 3, 28049 Madrid, Spain. ²ETSI de Telecomunicación, Universidad Rey Juan Carlos, Calle Tulipán, 28933 Madrid, Spain. [†]Current address: Departamento de Química Física, Universidad Complutense de Madrid, Avenida Complutense, 28040 Madrid, Spain. *n.case-lli@csic.es, #antonio.consoli@urjc.es, §c.lopez@csic.es

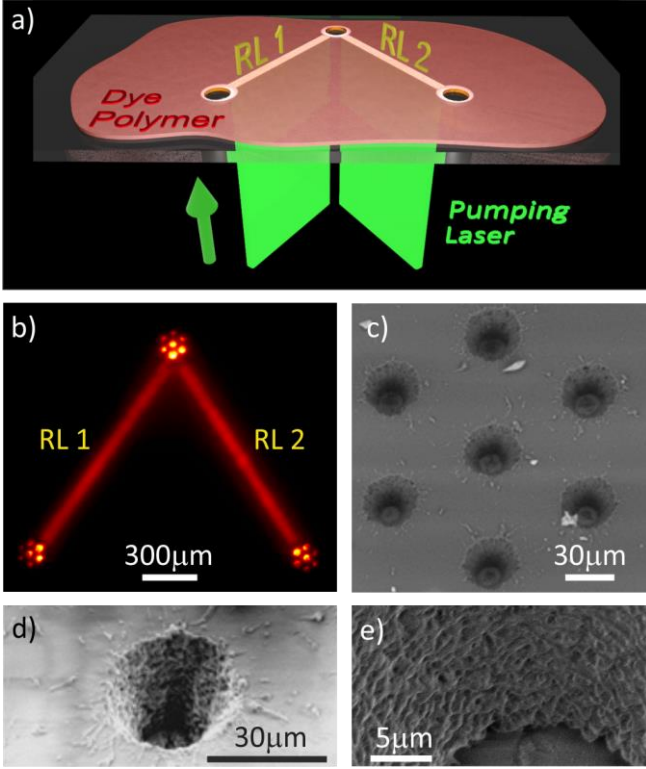


Figure 1. | RL network fabrication a) Schematics of the random lasers network. The dye-doped polymer thin film is deposited on a glass substrate and scattering centres are created by drilling the film. Optical excitation is performed by an SLM sculpted laser impinging from the bottom and uniformly pumping regions that connect the scatterers. b) Emission intensity image (acquired by CCD) of two RLs pumped simultaneously. Each resonator consists of a rectangular pumped volume placed between two scattering centres made of seven holes in a hexagonal pattern. c-e) Scanning electron microscopy (SEM) images of one of the scattering centres in b), reported with increasing magnification to highlight the rough sidewalls inside a given hole, responsible for the RL feedback action.

to extend the proposed approach to simulate neural networks.

Network preparation

For the sake of simplicity, before extending the study to more complex geometries, we focus on the basic building block of a network: two equivalent RLs connected through a node, consisting of a scattering centre that furnishes feedback sufficient for both random architectures to lase. In this configuration, we prove that one RL emission can be affected by the action of the second RL with which it has a scattering centre in common. In the networks under investigation, the way the amplified modes of a single RL are modified strongly resembles the mode interaction in a standard laser cavity with an external feedback^{27,28}. We realised different network archetypes of up to three RLs consisting of scattering centres with increasing complexity and proved that every investigated arrangement can sustain effective RL interactions.

The typical single RL we used, representing the building-block of RL networks, is composed of two distant (≈ 2 mm) scattering centres connected by a laser pumped stripe²⁵. When optical gain overcomes losses, amplified spontaneous emission, which is spectrally coupled with modes of the unconventional cavity, generates a RL. The

active medium in which the random lasing occurs is a solid, dye-doped biopolymer thin film (see Methods) in which the polymer matrix has been chosen for its ability to prevent dye quenching^{29,30}. The networks of RLs are realised by inscribing scattering centres by means of a direct laser-writing technique into the polymer film and by optically pumping the dye-polymer region through an ensemble of stripes projected on the sample surface (see the schematics of Fig. 1a, the out-of-plane emission shown in Fig. 1b and Methods).

Each scattering centre consists of a single (Fig. 1d,e) or a series of holes (diameter size about tens of μm), as those -arranged in a hexagonal pattern- reported in Fig. 1b-c. The rough internal surfaces of the drilled holes form a disordered air/polymer interface able to strongly scatter light coming from the pumped volume (see Fig. 1b), thus providing the feedback for lasing action. The number of laser modes sustained by a RL with spatially localized feedback, as well as their threshold and angular distribution, has been proven to depend on the roughness and porosity of the scattering surfaces^{31,32}.

The scattering centres act as disordered mirrors and, at the same time, as out-of-plane couplers, which allow to probe the lasing modes by recording the scattered emission orthogonally to the sample surface (see Methods). It is worth mentioning that random modes in this kind of RL with localized feedback emerge as stable sharp random spectral peaks (see Fig. S1-S3) and the same resonances are recorded in both scattering centres (see Fig. S2). This indicates that the device is acting as a single oscillator, supporting modes some of which enjoy sufficient gain to be amplified in the round-trip between the two scattering regions²⁴.

Measuring the coupling

When considering RL networks, one must establish a protocol to determine the existence of coupling on the basis of the spectra acquired from each or the compound resonator. Two different resonators measured independently provide spectra that can be taken as standard for independence (fully uncorrelated) whereas two spectra taken successively from a single resonator (only subject to stochastic fluctuations) can be used as standard for strong dependence and similarity, since high correlation is assured.

We started by addressing the simplest case consisting of two RLs having one scattering node in common. In this configuration, two resonators activated one at a time show distinct, uncorrelated spectra that we take as benchmark of spectral independence. When both RLs are pumped simultaneously, if they do interact (coupling through the common disordered mirror) the emerging spectral features must depend on the lasing state of both resonators. Several circumstances can be expected to occur such as frequencies common to both uncoupled resonators not belonging to the compound one, modes from some resonator becoming available to the compound one, modes not lasing in any resonator showing as a consequence of the coupling and, generally, changes in mode gain. This provides an alternative method to detect coupling between resonators: searching for dissimilarity between the spectrum of one when pumped alone and when in conjunction with the

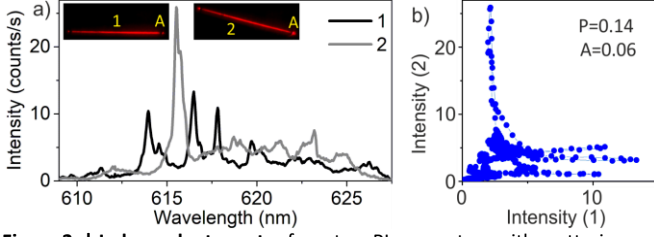


Figure 2. | Independent spectra from two RL resonators with scattering centres made of single holes of 30 μm diameter size as an example of fully uncorrelated spectra. a) Spectrum acquired in position A by pumping line 1 (black curve) and line 2 (grey curve), respectively. In the insets the out-of-plane emissions of the two cases are reported. Both lines length is 2 mm. b) Parametric plot of the intensity of the spectra reported in a). The values of Pearson correlation (P) and of the area of the parametric plot (A) are reported for each case.

other. The fingerprint of an effective interaction would thus be a spectral modification, *i.e.* peak wavelength-shifts and/or an intensity redistribution, that may be detected at every network node. Therefore, the *modus operandi* we followed to test mode coupling occurrence was acquiring spectra of each single RL (at the same sets of wavelengths) and compared them to the spectrum emerging from the simultaneous activation of both RLs in the network.

To set a standard for uncoupled cavity lasers we first studied the device reported in the inset of Fig. 2a, where two RLs (labelled 1 and 2) share the scattering centre A. The device is composed by three scattering nodes made of single holes connected by pumping lines. The two RL emissions (spectra 1 and 2) are expected to be independent, as they originate from two different cavities non-simultaneously activated and, as shown in Fig. 2a, they show two uncorrelated sets of peaks when acquired in the same position (A).

In order to visually highlight the low correlation and spectral difference between the two RLs, in Fig. 2b we reported the intensity of the first spectrum as a function of the intensity of the second one, for every acquired wavelength: each data point having coordinates $[I_1(\lambda_i), I_2(\lambda_i)]$ for $i = 1 \dots n$, with n corresponding to the number of wavelength data. This representation will be hereafter called parametric plot. Since in this picture the vast majority of data lay outside the diagonal line, a low linear correlation is evident, as quantified by the small value of the Pearson coefficient being $P = 0.14^{33,34}$. The high intensity peaks of one RL lying on background intensity regions in the other RL, appear as vertical and horizontal streaks, while data in fluorescence background regions of both resonators appear as a cloud at lower intensities. Obviously two proportional spectra would give a straight line in this kind of representation, with the Pearson correlation directly proportional to the regression coefficient.

An additional measure to assess the degree of similarity between spectra, can be provided by the area (A) enclosed by the lines that connect the parametric plot data. The area measure increases with shifted, overlapping peaks but, at variance with Pearson's correlation it attains very small values both for high correlation (*e.g.* between nearly proportional spectra, see SI) and very low correlation (vertical and horizontal streaks in Fig. 2b). Therefore, a high A value implies that the overlap is not complete, but

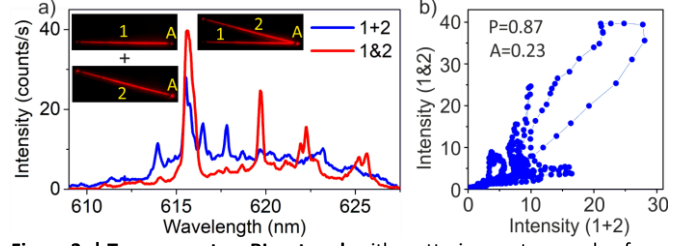


Figure 3. | Two resonators RL network with scattering centres made of single holes of 30 μm diameter size, corresponding to the one reported in Fig. 2. a) Spectra obtained by summing the single emissions (1+2, blue curve), and by pumping simultaneously both lines (1&2, red curve). All the spectra are detected in position A. b) Parametric plot of the intensity of the spectra reported in a). The values of Pearson correlation (P) and of the area of the parametric plot (A) are reported for each case.

that the spectra exhibit small variations in the peak positions and/or amplitudes, as occurs if an effective weak interaction was in place. In our analysis, it is the conjunction of the parameters P and A that allows to estimate the coupling between single RLs in the network. For instance, for the two independent RLs reported in Fig. 2a the low value of both parameters ($P = 0.14$ and $A = 0.06$) proves the negligible correlation between them.

When two resonators do couple, this interaction must appear as a difference between the sum of their independent spectra and the compound spectrum obtained with simultaneous pumping. We used the dissimilarity between added spectra from the involved resonators and the spectrum from the compound resonator as a smoking gun of coupling. When both RLs are simultaneously active, the compound spectrum (1&2), reported in Fig. 3a (red line), was acquired at the common scattering node, in order to overcome fluctuations in the out-of-plane emission between different nodes. This emission has to be compared to the sum of the separate spectra taken successively (1+2) at the same node, reported in Fig. 3a with blue line. If no interaction were taking place, each RL would independently scatter their emission out of the network and the compound emission would be the sum of the two single RL spectra, resulting in strong overlap and high correlation ($P \approx 1$; $A \approx 0$). The extreme opposite would lead to compound spectrum retaining no features from either resonator, thus bearing no resemblance with their sum, in which case a streaked parametric plot would result ($P \approx 0 \approx A$). A case where $P \approx 0$; $A \approx 1$ cannot occur for spiked spectra (or even background fluorescence) as it is a signature of fully random noise signal.

In Fig. 3a-b the sum spectrum shows a clear difference with the emission detected from the compound resonator, exhibiting lessened correlation, $P \approx 0.87$, and a moderate area $A \approx 0.23$. Typical values for correlation in successive acquisitions of one resonator emission (See Fig. S3) provide a benchmark for highly correlated spectra as high as $P \approx 0.98$. A redistribution of the spectral density with suppression and/or enhancement of existing modes, up to the occurrence of new ones, is observed. It is remarkable how the compound emission is dominated by two strongly enhanced peaks at 615.6 nm (giving rise to the large loop in the parametric plot, responsible for most of the value of A) and 619.7 nm (originating one large vertical streak), while the majority of the emission is inhibited with respect to the

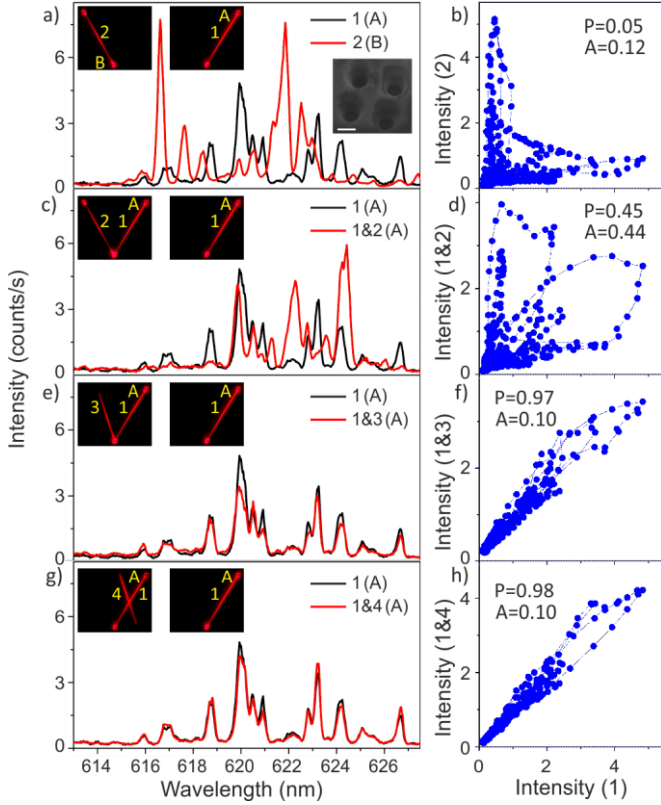


Figure 4. | RL network with scattering centres made of holes (50 μm diameter size) arranged in square pattern with 100 μm side. a) Spectrum acquired in position A by pumping line 1 (black curve) and in position B by pumping line 2 (red curve). In the insets the out-of-plane emission of the two RLs is reported, along with the SEM image of one scattering centre (scale bar 50 μm). b) Parametric plot of the intensity of the spectra reported in a). c) Spectra acquired in position A by pumping line 1 (black curve), line 1 and 2 simultaneously (1&2, red curve). d) Parametric plot of the intensity of the spectra reported in c). e) Spectra obtained in A by pumping line 1 (black curve) and line 1 and 3 simultaneously (1&3, red curve). f) Parametric plot of the intensity of the spectra reported in e). g) Spectra obtained in A by pumping line 1 (black curve) and line 1 and 4 simultaneously (1&4, red curve). h) Parametric plot of the intensity of the spectra reported in g). The values of Pearson correlation (P) and of the area of the parametric plot (A) are reported for each case.

sum spectrum. The emission stability of the RLs was checked in every spectral acquisition (see Method and SI) and the differences observed between the sum and the compound spectra cannot be ascribed to variations in the exciting conditions, polymer degradation or detection instabilities.

Investigation of many (≈ 20) network devices with the same design revealed that the spectral rearrangement occurs with large variations. We found fingerprint of coupling ($A > 0.15$ and $P < 0.9$) in 40% of the cases; while the interaction was poorly noticeable in the other cases (30% of cases with $0.10 < A < 0.15$; 30% with $A \leq 0.10$). This large inhomogeneity is the result of random variations in mode gain and coupling strength, which depends on the specific features of the resonators and on spectral and spatial overlap of random lasing modes, that are not controllable *a priori*. The analysis presented in this work aims to prove that individual RLs with localized feedback composing a network can exhibit mode coupling between them.

Apart from investigating the sum vs compound spectral similarity at the common node, another experimental ap-

proach worth studying to prove mode coupling is evaluating how one RL emission from nodes that are not shared is influenced by the network interaction. Moreover, to prove the universality of the coupling occurrence, we varied the geometry of the scattering centres by fabricating networks with three nodes, positioned at the corners of an equilateral triangle, each consisting of four holes arranged in a square pattern, as reported in the inset of Fig. 4a. Two single RLs are induced by pumping the lines that connect corners A-B (line 1) and B-C (line 2), respectively, as shown in Fig. 4a. The corresponding parametric plot demonstrates the low correlation between spectra from two independent single resonators excited successively ($P = 0.05$; $A = 0.12$). In order to test the influence of RL 2 on the emission of RL 1, spectra were collected from position A when RL 2 was (Fig. 4c red line) or was not pumped (Fig. 4c black line). In this position the emission of RL 2 alone is null in the absence of RL 1 action (see SI), so that, trivially, the sum 1+2 equals the emission of RL 1. When RL 2 was turned on, new modes got amplified through line 1 and were observed in node A, for instance those at 608 nm and 623 nm, which belong to the emission of RL 2. At the same time, some modes experienced a suppression, like those at 614 nm and 616 nm. The parametric plot, reported in Fig. 4d, furnishes a heavily reduced linear correlation, $P = 0.45$, and a high area value, $A = 0.44$, thus bearing evidence of a strong interaction between the two RLs.

To check the reliability of the method in addressing the RLs coupling, we studied the modification induced on the emission of RL 1 by the presence of a pumping line that does not constitute a RL (line 3 in Fig. 4e does not end in a second backscattering centre) or that does not even share any scattering centre with RL 1 (line 4 in Fig. 4g). These cases are reported in Fig. 4e-h and constitute examples of high correlation ($P \approx 0.97$) and low area parameter ($A \approx 0.1$) proving how a pumping line not belonging to the network does not affect the emission of the RL considered. Further examples are reported in the SI.

Ring network

A RL network still simple yet more complex than the one investigated in Fig. 4, was considered too. It consists of three scattering centres made of 7 holes arranged in hexagonal pattern (see Fig. 1b-e). Here, we exploited all three single RLs emerging by pumping the device with lines connecting the scattering centres. When all single RLs are pumped, the spectral fingerprint collected at each node position show high correlation (see SI, Fig.S12), proving that the system can be considered a unique, compound resonator with delocalized modes (not associated to a particular resonator). We focused on the effect induced by switching on/off a single RL of the network. In particular, the network emission variation induced by turning on the pumping line B-C (RL 3) is reported in Fig. 5a-b. The emission extracted from A (that does not belong to RL 3), was strongly modified by the action of the random modes of RL 3. The analysis of the parametric plot of the spectra collected when i) only lines 1 and 2 are pumped and ii) the three lines are pumped at the same time, gives $P = 0.43$ and $A = 0.32$, indicating a strong spectral modification

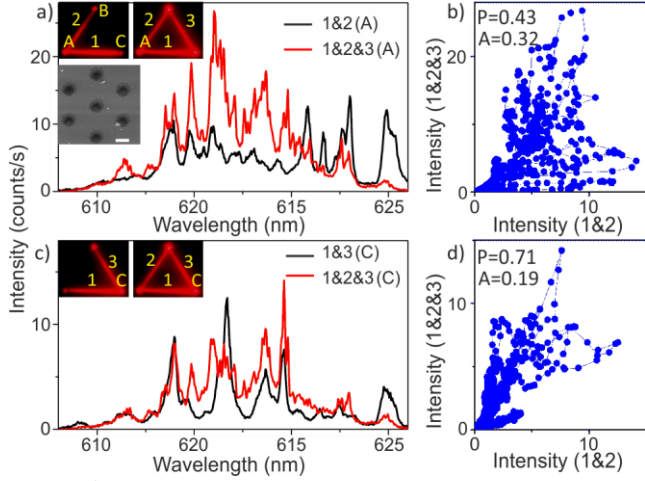


Figure 5. | Ring RL network with scattering centers made of holes (diameter size of 30 μm) arranged in hexagonal pattern. a) Spectrum acquired in position A by pumping lines 1 and 2 (1&2, black curve), and by pumping all the lines at the same time (1&2&3, red curve). In the insets the corresponding out-of-plane emissions are reported, along with the SEM image of one scattering center (scale bar 30 μm). b) Parametric plot of the intensity of the spectra reported in a). c) Spectra acquired in position C by pumping lines 1 and 3 (1&3, black curve), and by pumping all the lines (1&2&3, red curve). d) Parametric plot of the intensity of the spectra reported in c). The values of Pearson correlation (P) and of the area of the parametric plot (A) are reported for each case.

that, again, produces a reduced correlation and a high enclosing area. In this case the coupling fingerprints are due to the spikiness of the spectra causing small wavelength shifts and large intensity variations, which contribute to the formation of many loops in the parametric plot. A similar behaviour, although resulting in a weaker interaction ($P = 0.71$ and $A = 0.19$), is found by measuring in C the effect of switching RL 2, reported in Fig. 5c-d. Comparison between the three scattering centres morphologies presented in this work shows that larger holes number, i.e. increased disorder surfaces, boost the chances to establish coupling.

The analysis based on the conjunction of the Pearson's correlation and the enclosed area allowed to quantify the coupling in a network of RLs with localized feedback, since the interaction induces a spectral redistribution of the amplified modes. With respect to other method that evaluate the similarity between different spectra, such as the auto-correlation function³⁵ or the mutual information³⁶ our method gives a remarkable outcome in highlighting spectral redistributions [see SI].

Numerical model

In order to substantiate the experimental findings we simulated the random lasers network in the framework of coupled mode theory^{37,38}. We first created a large pool of 40 modes, from which a RL was assigned 10 modes ($j, k = 1 \dots 10$, randomly chosen among the globally defined, see Methods), which satisfy a time dependent set of differential equations:

$$\dot{a}_k = i\omega_k a_k - \alpha_k a_k + \sum_{j \neq k} c_{j,k} a_j + g(t, \omega_k) \frac{a_k}{1 + \gamma_k |a_k|^2} \quad (1)$$

where $a_k(t)$ is the complex amplitude of the k -th mode as a function of time, ω_k the frequency, α_k the losses, $c_{j,k} \propto |\omega_k - \omega_j|$ the coupling coefficient with all other j -th modes

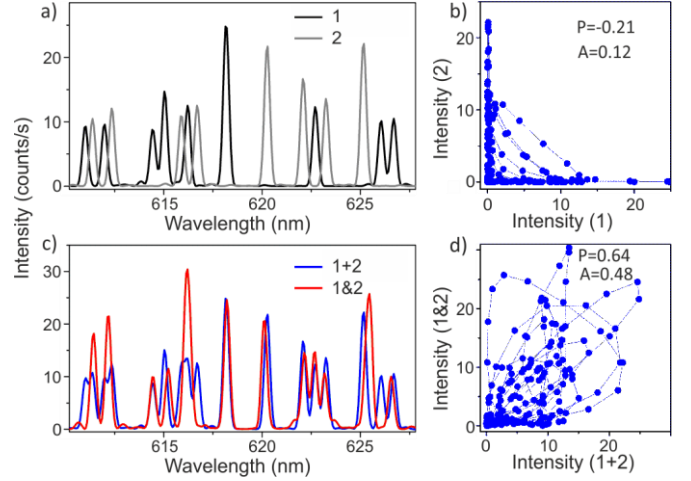


Figure 6. | Numerical simulation employing coupled mode theory. a)-b) Spectra corresponding to two independent RLs, black and gray curves in a), show a low correlation in the parametric plot in b). c) The sum of the spectra in a) (1+2, blue line) is compared to the spectrum (1&2, red line) obtained by introducing a coupling term between the two sets of modes. d) The parametric plot of the spectra in c) shows an intermediate value of P and a high area parameter, evidence of a RL modes interaction.

that fade with detuning, $g(t, \omega_k)$ the time dependent mode gain (pump pulse) and γ_k the gain saturation coefficient. Eq. (1) describes how the k -th mode evolves in time. By Fourier transforming the solution, we obtained the spectral profile in amplitude and phase of each mode and the full spectrum is retrieved by summing the intensity of all modes. In this way, two independent RLs are represented by two sets of 10 modes randomly chosen from the pool, for which Eq. (1) is solved separately, that is, couplings are only considered within the 10-sets giving rise to the grey and black spectra reported in Fig. 6a, respectively. Notice that, due to the coupling, not all modes necessarily show in the spectrum, having merged with neighbouring ones. The parametric plot of Fig. 6b, heavily dominated by vertical and horizontal streaks, highlights the very low correlation between them, exhibiting $P = -0.21$ and $A = 0.12$.

In modelling the case of two coupled RLs, Eq. (1) was solved considering that the two 10-sets of modes owned by each resonator entered the equation, as they were pumped at the same time. In this case, modes belonging to different sets were randomly interleaved and subject to coupling. The resulting compound spectrum, 1&2, (red line in Fig 6c) was compared to the sum of the single resonators, 1+2 (black line in Fig. 6c). The coupling gave rise to a sizable spectral redistribution with respect to the sum of the stand-alone emissions. In fact, the frequency and intensity of the peaks are slightly changed, with attraction/repulsion between adjacent modes and energy transfer due to the mode interaction. The corresponding parametric plot of Fig. 6d shows a reduced value for the linear correlation ($P = 0.64$) along with a high area parameter ($A = 0.48$), closely resembling the experimental observations reported in Fig. 3d, Fig. 4b and Fig. 5d. This demonstrates that in the presence of an effective interaction, the spectra show a reduced linear correlation along with a high area value, as we found experimentally.

To summarize, we realized multiple random lasers featuring spatially localized feedback in a planar morphology by inscribing scattering centres in a film of gain material

made of dye-doped biopolymer and spatially selective pumping the line joining them. By designing networks in which random lasers share scattering centres, we proved that it is possible to induce an effective coupling between them. Spatially resolved probing allowed to spectrally detect their interaction. By correlation analysis we proved that random lasers can interact as a synchronous ensemble and behave as coupled oscillators. Our findings are supported by coupled modes theory calculations that predict the observed spectral correlations. The presented architecture has a small footprint, low fabrication complexity and cost, making it a good candidate to study highly nonlinear interactions in networks. We believe that the ample potential for large connectivity and synaptic plasticity offered by this platform will trigger the study of more complex networks based on random lasers aiming to realize photonic neural network architectures. Finally, this can be an initial step in developing statistical methods based on machine learning in order to address and evaluate the RL interaction even in more complex network geometries.

ACKNOWLEDGEMENTS

This work was partially funded by the Spanish MCIU RTI2018-093921-B-C41 project. N. C. acknowledges MCIU *Juan de la Cierva* program. Álvaro Blanco is thankfully recognised for fruitful discussions.

METHODS

Sample preparation

The dye-doped biopolymer films were produced by introducing 4-(dicyanomethylene)-2-methyl-6-(4-dimethylaminostyryl)-4H-pyran (DCM) molecules, with a 0.35% mass concentration in a deoxyribonucleic acid (DNA)-cetyltrimethyl ammonium (CTMA) polymer matrix. The cationic surfactant CTMA (Sigma-Aldrich 292737) was used to make the DNA (Sigma-Aldrich D1626) soluble in organic solvents and then easily mixable with the DCM dye-molecules solution. The DNA-CTMA complex is dissolved (4 vol.%) in ethanol and mixed with the DCM solution (0.5 vol.% in equal parts of ethanol and chloroform). The resulting blend was magnetically stirred for 5 hours. Then it was spread by dropcasting onto a glass substrate, and solid films with a thickness of about 20 μm were obtained after drying the sample at room temperature and pressure.

The scattering centres that serve as disordered mirrors and provide localized feedback for RL were fabricated by using a direct laser-writing technique. The polymer was locally ablated by means of a short-pulsed (100 fs), high-energy ($\sim 250 \mu\text{J}/\text{pulse}$) Ti:Sapphire laser emitting at 800 nm peak wavelength. The laser power, the number of shots delivered and the focusing position were controlled by using a half-wave plate retarder in conjunction with a linear polarizer, a software controlling the laser output and motorized translational stages, respectively. A single laser shot focused by a lens of 5 cm focal length drilled a hole in the polymer matrix. In order to create a reproducible hole size, we overcame the shot-to-shot laser power fluctuations by lowering power and increasing the number of pulses (50 single shots) delivered to obtain each hole. This assures that, in the energy range between 200-300 $\mu\text{J}/\text{pulse}$, the local ablation removed completely the polymer and reached the underlying glass substrate, thus leaving a cylindrical-like air-defect in the polymer matrix. By varying the laser fluence we achieved reproducible holes with diameter size in the range 30-150 μm .

Random lasers measurements

The excitation setup involves a 10 ns pulsed, frequency doubled 532 nm Nd:YAG laser with a 10 Hz repetition rate, whose beam was shaped by an amplitude spatial light modulator working in reflection. By means of this scheme we imaged on the sample surface the intensity distribution required to produce the desired optical pumping geometry. We drew a set of stripes of same length and width (50-100 μm) connecting scattering centres, as reported in Fig. 1a-b. The out-of-plane lasing emission was imaged with a magnification equal to 2 both on a CCD, see Fig. 1b, and on a plane where an optical fibre tip connected to a spectrometer collected the signal, which was coupled to a spectrometer and a visible light detector (SPEC, Andor Shamrock 303). We achieved a spatial and spectral resolution of 50 μm and 0.1 nm, respectively. The fibre tip was mounted on motorized translation stages in order to collect the radiation emerging from different scattering centres. It is important to stress that by applying this pumping scheme, and by triggering the spectral acquisition to the laser repetition rate, consecutive spectra are independent from one another. In order to prove the stability during the entire acquisition time, we repeated a sequence of illumination frames, each of which contains a different pumping lines configuration in the network. For instance, referring to Fig. 2 the sequence was composed by three frames: line 1, line 2, lines 1&2. For each frame we acquired 50 consecutive spectra, corresponding to 50 laser single shots, to be averaged. The sequence was repeated many times. Therefore, for each illumination geometry we achieved a series of nominally identical spectra mixed in time. In every series the spectral fluctuations were minimal, exhibiting a high degree of correlation ($P = 0.98$ on average, see SI) over a period of about 5 min. After longer times of constant exposition above laser threshold, the polymer matrix suffered modifications due to the induced heating, hence causing the spectrum to slowly change and to experience a correlation decrease with respect to the initial one that usually led to a complete decorrelation after 15 min (see SI). On grounds of such stability analysis, for every investigated RL configuration we performed a series of ten nominally identical acquisitions, averaged to obtain a reliable spectral signature. More details concerning pumping threshold, integration time and stability can be found in the SI.

Numerical model.

The system under investigation was numerically replicated by a set of $N = 40$ random possible lasing frequencies, almost evenly spaced (a 5% degree of fluctuation from equispaced was added) in order to cover the spectral range of interest. The excitation pulse was designed to reproduce the pump used in experiments with about 10 ns and a gain bandwidth of about 30 nm. The gain saturation coefficient γ_k was considered equal for all modes. The coupling coefficient matrix $c_{j,k}$ in Eq. (1) was defined for all modes by assigning decreasing real values for increasing mode spectral detuning, with a linear slope. The maximum value of the coupling was chosen as $c_{\text{max}} = 1.5 \cdot 10^{-5} (g_{\text{max}} - \alpha_{\text{max}})$. The same coupling matrix was used for calculating the spectra of the single resonators and of the coupled compound where all the modes interact simultaneously through $c_{j,k}$. In order to simulate the experimental lasing spectra, we considered that in each single RL 10 different modes (randomly selected among the N possible) are allowed to lase. The introduction of mode coupling implies that the instantaneous frequency of the k -th mode, defined as the time derivative of the phase, varies with respect to its initial value, ω_k as a function of time, depending on the coupling to other modes. This effect explains the frequency shift from ω_k , so that adjacent modes can partially overlap until, in the limit of high coupling, a single peak emission is found. In the framework of coupled mode theory, the peak modification is due to energy exchange in time between interacting modes.

Data availability

The data that support the plots within this paper and other findings of this study are available from the corresponding authors upon reasonable request.

Code availability

The MATLAB codes developed to execute the calculations presented in this paper are available from the corresponding authors upon reasonable request.

REFERENCES:

1. Pikovsky, A., Rosenblum, M. & Kurths, J. Synchronization: a Universal Concept in Nonlinear Sciences. (Cambridge: Cambridge University Press, 2001).
2. Arenas, A., Díaz-Guilera, A., Kurths, J., Moreno, Y. & Zhou, C. Synchronization in complex networks. *Phys. Rep.* 469, 93–153 (2008).
3. Boccaletti, S., Kurths, J., Osipov, G., Valladares, D.L., Zhou, C. S. The synchronization of chaotic systems. *Phys. Rep.* 366, 1–101 (2002).
4. S.H. Strogatz, D. M. Abrams, A. McRobie, B. Eckhardt, E. O. Crowl synchrony on the Millennium Bridge. *Nature* 483, 43–44 (2005).
5. Kolodner, P., Slimani, S., Aubry, N. & Lima, R. Characterization of dispersive chaos and related states of binary-fluid convection. *Phys. D Nonlinear Phenom.* 85, 165–224 (1995).
6. Hansel, D., Mato, G. & Meunier, C. Phase dynamics for weakly coupled hodgkin-huxley neurons. *Epl* 23, 367 (1993).
7. Ohtsubo, J. Semiconductor Laser Networks: Stability, Instability and Chaos, Ch 14. (Atlanta: Springer Series in Optical Sciences, 2017).
8. Heil, T., Fischer, I., Elsässer, W., Mulet, J. & Mirasso, C. R. Chaos synchronization and spontaneous symmetry-breaking in symmetrically delay-coupled semiconductor lasers. *Phys. Rev. Lett.* 86, 795–798 (2001).
9. Zhang, Q., Yu, H., Barbiero, M., Wang, B. & Gu, M. Artificial neural networks enabled by nanophotonics. *Light Sci. Appl.* 8, (2019).
10. Terry, J. R. et al. Synchronization of chaos in an array of three lasers. *Phys. Rev. E - Stat. Physics, Plasmas, Fluids, Relat. Interdiscip. Top.* 59, 4036–4043 (1999).
11. Liu, Y. et al. Experimental observation of complete chaos synchronization in semiconductor lasers. *Appl. Phys. Lett.* 80, 4306–4308 (2002).
12. Montinaro, M. et al. Diverse Regimes of Mode Intensity Correlation in Nanofiber Random Lasers through Nanoparticle Doping. *ACS Photonics* 5, 1026–1033 (2018).
13. Höfner, M., Wünsche, H. & Henneberger, F. A random laser as a dynamical network. *New J. Phys.* 16, 033002 (2014).
14. Krämmer, S. et al. Random-Cavity Lasing from Electrospun Polymer Fiber Networks. *Adv. Mater.* 26, 8096–8100 (2014).
15. Wiersma, D. S., Bartolini, P., Lagendijk, A. & Righini, R. Localization of light in a disordered medium. *Nature* 390, 671–673 (1997).
16. Cao, H. et al. Random laser action in semiconductor powder. *Phys. Rev. Lett.* 82, 2278–2281 (1999).
17. Cao, H. et al. Ultraviolet lasing in resonators formed by scattering in semiconductor polycrystalline films. *Appl. Phys. Lett.* 73, 3656–3658 (1998).
18. Redding, B., Choma, M. a. & Cao, H. Speckle-free laser imaging using random laser illumination. *Nat. Photonics* 6, 355–359 (2012).
19. Boschetti, A. et al. random laser. *Nat. Photonics* 14, 177–182 (2020).
20. Vynck, K., Burresi, M., Riboli, F. & Wiersma, D. S. Photon management in two-dimensional disordered media. *Nat. Mater.* 11, 7–12 (2012).
21. Cui, L. et al. Retrieval of contaminated information using random lasers. *Appl. Phys. Lett.* 106, (2015).
22. Ignesti, E. et al. A new class of optical sensors: a random laser based device. *Sci. Rep.* 6, 35225 (2016).
23. Wang, Y. et al. Random lasing in human tissues embedded with organic dyes for cancer diagnosis. *Sci. Rep.* 7, 1–7 (2017).
24. Consoli, A. & López, C. Decoupling gain and feedback in coherent random lasers: experiments and simulations. *Sci. Rep.* 5, 16848 (2015).
25. Consoli, A. & Lopez, C. Emission regimes of random lasers with spatially localized feedback. *Opt. Express* 24, 10912 (2016).
26. Jiang, X., Cao, H., Ling, Y., Xu, J. Y. & Soukoulis, C. M. Mode repulsion and mode coupling in random lasers. *Phys. Rev. B - Condens. Matter Mater. Phys.* 67, 1–4 (2003).
27. Biasco, S. et al. Frequency-tunable continuous-wave random lasers at terahertz frequencies. *Light Sci. Appl.* 8, 1–13 (2019).
28. Liu, Y., Ohtsubo, J. & Ye, S. Y. Dynamical and coherent characteristics of semiconductor lasers with external optical feedback. *Proc. SPIE - Int. Soc. Opt. Eng.* 2886, 120–127 (1996).
29. Steckl, A. J. DNA – a new material for photonics? *Nat. Photonics* 1, 3–5 (2007).
30. Leonetti, M., Sapienza, R., Ibisate, M., Conti, C. & López, C. Optical gain in DNA-DCM for lasing in photonic materials. *Opt. Lett.* 34, 3764 (2009).
31. Consoli, A. & López, C. Lasing optical cavities based on macroscopic scattering elements. *Sci. Rep.* 7, 40141 (2017).
32. Consoli, A., Soria, E., Caselli, N. & López, C. Random lasing emission tailored by femtosecond and picosecond pulsed polymer ablation. *Opt. Lett.* 44, 518 (2019).
33. Pearson, K., Filon, L. N. G. Mathematical Contributions to the Theory of Evolution . IV . On the Probable Errors of Frequency Constants and on the Influence of Random Selection on Variation and Correlation. *Philos. Trans. R. Soc. London. Ser. A, Contain. Pap. a Math. or Phys. Character* 101, 229–311 (1898).
34. Rodgers, J. L. & Nicewander, W. A. Thirteen Ways to Look at the Correlation Coefficient. *Am. Stat.* 42, 59–66 (1988).
35. De Gelder, R., Wehrens, R. & Hageman, J. A. A Generalized Expression for the Similarity of Spectra: Application to Powder Diffraction Pattern Classification. *J. Comput. Chem.* 22, 273–289 (2001).
36. Kraskov, A., Stögbauer, H. & Grassberger, P. Estimating mutual information. *Phys. Rev. E - Stat. Physics, Plasmas, Fluids, Relat. Interdiscip. Top.* 69, 16 (2004).
37. Haus, H. A. Mode-locking of lasers. *IEEE J. Sel. Top. Quantum Electron.* 6, 1173–1185 (2000).
38. Conti, C., Leonetti, M., Fratalocchi, A., Angelani, L. & Ruocco, G. Condensation in disordered lasers: Theory, 3D+1 simulations, and experiments. *Phys. Rev. Lett.* 101, 2–5 (2008).